SCIENCE CHINA
Information Sciences

• RESEARCH PAPER •

August 2022, Vol. 65 182202:1–182202:15
https://doi.org/10.1007/s11432-020-3074-5

Active model-based nonlinear system identification of quad tilt-rotor UAV with flight experiments

Zhong LIU[1*], Didier THEILLIOL[2], Yuqing HE[3,4], Feng GU[3,4], Liying YANG[3,4] & Jianda HAN[3,4,5]

[1]*Xi'an Modern Control Technology Research Institute, Xi'an* 710065*, China;*
[2]*Faculte des Sciences et Techniques, CRAN UMR 7039, CNRS, University of Lorraine, Vandoeuvre-les-Nancy* 54506*, France;*
[3]*State Key Laboratory of Robotics, Shenyang Institute of Automation, Chinese Academy of Sciences, Shenyang* 110016*, China;*
[4]*Institutes for Robotics and Intelligent Manufacturing, Chinese Academy of Sciences, Shenyang* 110169*, China;*
[5]*College of Artificial Intelligence, Nankai University, Tianjin* 300350*, China*

Received 8 June 2020/Revised 26 July 2020/Accepted 1 September 2020/Published online 27 July 2022

Abstract To propose an accurate and less complex model of a special unmanned aerial vehicle (UAV), namely tilt-rotor UAV (TRUAV), this study identifies the active model-based nonlinear system of a quad-TRUAV. First, a nominal nonlinear model of the vehicle is formulated. Some unstructured nonlinearities are ignored to reduce the complexity of the model. Then, due to the unstable dynamics of the open-loop system, the format of this nominal model is considered to design an innovative smooth-switch attitude control via interconnection and damping assignment passivity-based control (IDA-PBC). Active model-based nonlinear system identification is studied for the vehicle with the designed control method and flight experiments. The model error vector is defined and estimated by the unscented Kalman filter (UKF) to improve the accuracy of the model. The main contribution of this paper is to identify the nominal nonlinear model and to develop an active model method of the quad-TRUAV. The attitude control method with an innovative smooth-switch structure is another contribution to flight experiments. Numerical results are displayed to present the experimental results and effectiveness of the proposed nonlinear models.

Keywords tilt-rotor, unmanned aerial vehicle, flight control, nonlinear system identification, active model method, unscented Kalman filter

Citation Liu Z, Theilliol D, He Y Q, et al. Active model-based nonlinear system identification of quad tilt-rotor UAV with flight experiments. Sci China Inf Sci, 2022, 65(8): 182202, https://doi.org/10.1007/s11432-020-3074-5

1 Introduction

Due to limitations of typical unmanned aerial vehicles (UAVs) such as rotorcraft UAVs (RUAVs) and fixed-wing UAVs (FWUAVs), tilt-rotor UAVs (TRUAVs) become a popular aircraft [1]. TRUAVs are equipped with tiltable rotors and own helicopter mode (vertical rotors) and airplane mode (horizontal rotors) to integrate capabilities of hovering and high-speed cruise. The dynamics of TRUAVs is similar to RUAVs and FWUAVs in these two flight modes. During the transition procedure between helicopter and airplane modes, the structure and dynamics of TRUAV vary with the rotor-tilt angle.

TRUAV aerodynamics is a complex combination of wings and rotors. Especially near the helicopter mode, the rotor downwash interacts with wings and airframe affecting the lift of the wing and thrust of the rotor [1]. In addition, the varying structure of a TRUAV changes the center of gravity (COG) and rotational inertia. Several lookup tables and complex aerodynamic calculations are required to represent the above items accurately. There are typical applications to large tilt-rotor aircraft [2,3] or TRUAVs with simulation and measurement tools [4,5], and established nonlinear models are mathematically complex. In flight control designs, several references, such as [6,7], prefer to identify the linear models and establish the linear state-space equations of TRUAVs in helicopter mode. To further describe the varying dynamics of

* Corresponding author (email: liuzhongjob@163.com)

the transition procedure, Refs. [8,9] identified the nonlinear models of tri-TRUAVs, and model mismatches exist with the applied offline system identification methods [10].

The nonlinear models of TRUAVs [4, 5, 8, 9] always provide the crucial basis for flight control, especially during the transition procedure. For example, Refs. [11,12] designed gain scheduling (GS) control methods with smooth-switch structure for TRUAV transition control, and the nonlinear model is required for the tilt corridor to limit flight velocity for safe velocity control [13]. Moreover, Refs. [14, 15] considered nonlinear control methods for TRUAVs and require accurate nonlinear models for applied control inputs and dynamic inversion. In the terms of control design and stability analysis, rational nonlinear models have to compromise accuracy and complexity. However, current TRUAV models seldom focus on this point, and are usually dramatically complex [4, 5] or obviously approximate limiting applications [6–9] of some control methods to some extent. Thus, in TRUAV control designs, a nonlinear model with excellent accuracy and acceptable complexity deserves attention and motivates this study.

To identify the nonlinear model of the quad-TRUAV, the present study simplifies the model formulation with some modeling assumptions to reduce the complexity of the model and formulates a nominal nonlinear model. Because of the open-loop unstable dynamics of the quad-TRUAV, the basic flight control method is first designed with this nominal model for the attitude stability. The interconnection and damping assignment passivity-based control (IDA-PBC) is inherently robust against dynamic disturbances [16]. Consequently, an improved version applies to design the attitude control method [17] and allows two attitude controllers to switch smoothly as GS methods. This smooth switch depends on the rotor-tilt angle, and the attitude stability of the quad-TRUAV during the transition procedure can be ensured based on passivity. Therefore, this method is superior to existing GS methods [11, 12]. Current GS methods are usually based on heuristic knowledge and take little consideration of stability conditions.

Unknown parameters of the above nominal model are estimated offline using ground and flight tests with the designed attitude control. Due to the linear dependence of these parameters, the least squares (LS) estimation approach, which is widely used in linear or nonlinear models offline [18, 19], is considered to identify the nominal model of the quad-TRUAV. To further improve the accuracy of the model, the active model method is developed by defining additional model errors to accommodate all model mismatches. This method can improve the accuracy by slightly increasing the complexity of the model. This is validated by the active model-based system identification of different UAVs [20, 21], artificial muscles [22], and unmanned surface vehicles [23]. Unlike some offline methods, the active model method estimates model errors online using estimators suitable for nominal linear or nonlinear models such as the Kalman filter [20–22] and unscented Kalman filter (UKF) [23]. UKF is applied to the study of the second-order accuracy [24] to address the nonlinearity of the TRUAV nominal model and make accurate estimations.

Compared to the existing studies, the contribution of this paper consists of three aspects:

(1) The nonlinear model of a quad-TRUAV system is identified in the present study. Compared to linear models [6, 7], the nonlinear model can describe the dynamics of the transition procedure with some accuracy and is regarded as the nominal model of the active model method.

(2) To further improve the accuracy of the model, the active model method is developed using UKF to identify the TRUAV model. Compared to the complex models with necessary tools [4,5] and approximate models with offline system identification methods [8, 9], the established nonlinear model compromises the accuracy and complexity of the model and is useful for further study of controller design.

(3) A superior and innovative smooth-switch attitude control method is designed for quad-TRUAV flight experiments using the simplification and IDA-PBC. Compared to existing GS methods [11,12], the designed attitude control method ensures the transition stability based on passivity.

The remaining sections of this paper are organized as follows. Section 2 introduces the quad-TRUAV system and formulates its nominal model with modeling assumptions. For closed-loop flight experiments, Section 3 simplifies the nominal model format and uses IDA-PBC to design the attitude control. The active model-based nonlinear system identification of the quad-TRUAV is introduced in Section 4. This includes ground and flight tests for parameter estimations and the active model method for model errors. Flight experiments and the effectiveness of the proposed quad-TRUAV model are presented in Section 5.

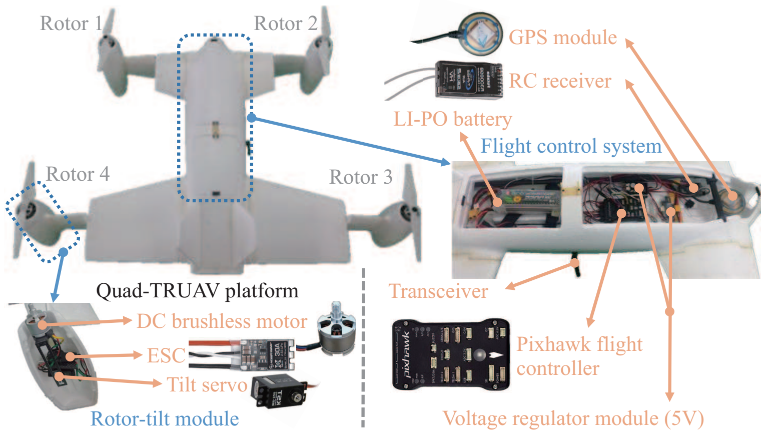

Figure 1 (Color online) Quad-TRUAV platform and system structure.

Table 1 Some structural parameters of quad-TRUAV platform

Parameter	Value
Mass (m)	1.615 kg
Mass of rotor-tilt module	0.15 kg
Wingspan ($\overline{b}$)	0.357 m (forward), 0.654 m (backward)
Wing area (S)	0.187 m^2
Average wing chord length ($\overline{c}$)	0.185 m
Longitudinal distances from rotors to COG (x_{rf}, x_{rb})	0.26 m (forward), 0.24 m (backward)
Lateral distances from rotors to COG (y_{rf}, y_{rb})	0.31 m (forward), 0.46 m (backward)
Inertias in three directions (helicopter mode) (I_{xx}, I_{yy}, I_{zz})	0.106 $\mathrm{kg\cdot m^2}$, 0.087 $\mathrm{kg\cdot m^2}$, 0.175 $\mathrm{kg\cdot m^2}$
Inertias in three directions (airplane mode) (I_{xx}, I_{yy}, I_{zz})	0.105 $\mathrm{kg\cdot m^2}$, 0.078 $\mathrm{kg\cdot m^2}$, 0.180 $\mathrm{kg\cdot m^2}$
Product of inertia in x-z plane (helicopter mode) (I_{xz})	0.007 $\mathrm{kg\cdot m^2}$
Product of inertia in x-z plane (airplane mode) (I_{xz})	0.005 $\mathrm{kg\cdot m^2}$
Stalling speed	Around 7 m/s

2 Quad-TRUAV system and model formulation

2.1 Quad-TRUAV platform and structure

The TRUAV in this study includes four tiltable rotors, as shown in Figure 1. The structure of this platform is similar to the V-44 airplane. Since the platform has no aileron, elevator, or rudder, four rotor-tilt angles are separately controlled by tilt servos with pulse width modulation (PWM) signals. The rotors of four direct-current (DC) brushless motors provide thrusts, and the speeds of rotors are regulated by electronic speed controllers (ESCs) with PWM signals. Some structural parameters of the quad-TRUAV are listed in Table 1. Here, bifilar pendulum experiments are performed for the values of rotational inertias and the product of inertia in the x-z plane [25]. These values are different in different flight modes.

Due to the unstable dynamics of quad-TRUAVs in the open loop, flight experiments require a flight control system for stabilization. As shown in Figure 1, a Pixhawk flight controller is applied in this quad-TRUAV system, which includes an inertial measurement unit (IMU) and magnetic compass for attitude information. A global position system (GPS) module is equipped as a separate onboard sensor for position information. The quad-TRUAV system is equipped with a remote control (RC) receiver and transceiver for receiving flight instructions from the ground control station and sending real-time messages. In the flight control system above, the flight control method will be designed in Subsection 2.2.

2.2 Nominal model of quad-TRUAV

Based on previous explanations, it is difficult to formulate some nonlinearities of the quad-TRUAV such as aerodynamic interactions and changes in structural parameters. To avoid considering these items

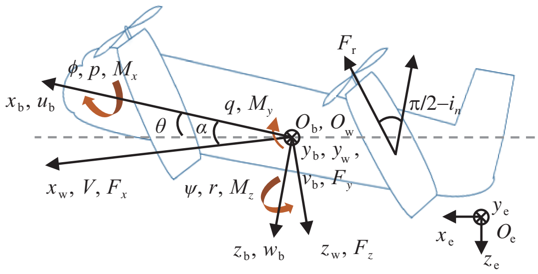

Figure 2 (Color online) Definitions of coordinate systems and states.

directly in complex aerodynamic calculations or lookup tables, modeling assumptions are introduced as follows: (1) Compared to the mass and rotational inertias of the quad-TRUAV, the mass and rotational inertias of the rotor-tilt module is negligible. (2) Rotational inertias of the quad-TRUAV are considered invariant in different flight modes. (3) The COG and center of aerodynamics are consistent and immobile with different rotor-tilt angles. (4) External interferences and aerodynamic interactions between rotors and aerodynamic components can be provisionally ignored in the simplified model formulation. (5) The rotor speed derived from the flight velocity can also be ignored.

According to the parameters listed in Table 1, the rotor-tilt module has a small mass, and the inertia of the quad-TRUAV does not change dramatically in various flight modes with less than 3% change in rotational inertias in x- and z-directions. Although the rotational inertia in the y-direction and product of inertia in the x-z plane vary by more than 10% in different flight modes, the induced model mismatches are still limited in normal flight conditions. Therefore, assumptions (1)–(3) can be inferred to be valid for the approximate model format. The quad-TRUAV is simplified as a typical rigid body with tiltable rotor thrusts and inevitable model mismatches. In addition, assumptions (4) and (5) are ideal and considered to further reduce the complexity of the model. With these two assumptions, complex aerodynamic interferences are ignored, and rotor models are considered invariant at different flight velocities. Based on all assumptions, the formulation of the quad-TRUAV model can be simplified. However, the established nominal model is approximate due to model mismatches similar to [8, 9]. Some methods need to regain ignored nonlinearities and improve the accuracy of the model.

To formulate the quad-TRUAV nominal model, some coordinate systems are defined in Figure 2, including the north-east-down (NED) coordinate system $O_\mathrm{e}x_\mathrm{e}y_\mathrm{e}z_\mathrm{e}$, body-axis coordinate system $O_\mathrm{b}x_\mathrm{b}y_\mathrm{b}z_\mathrm{b}$, and wind-axis coordinate system $O_\mathrm{w}x_\mathrm{w}y_\mathrm{w}z_\mathrm{w}$ [26]. Based on these coordinate systems, some states are defined, including flight velocity V and angle of attack α, as shown in Figure 2. With $[u_\mathrm{b}\ v_\mathrm{b}\ w_\mathrm{b}]^\mathrm{T}$ as the velocities in $O_\mathrm{b}x_\mathrm{b}y_\mathrm{b}z_\mathrm{b}$, the above states are in the forms $V = \sqrt{u_\mathrm{b}^2 + v_\mathrm{b}^2 + w_\mathrm{b}^2} > 0$, $\alpha = \arctan(w_\mathrm{b}/u_\mathrm{b})$, and angle of sideslip $\beta = \arcsin(v_\mathrm{b}/V)$. For Euler angles $[\phi\ \theta\ \psi]^\mathrm{T}$, $[p\ q\ r]^\mathrm{T}$ represent the corresponding attitude rates. Other symbols in Figure 2 will be explained in the following contents.

Similar to the model formulation of fixed-wing aerial vehicles, the longitudinal and lateral dynamic and kinematic equations of the quad-TRUAV are formulated as follows [26]:

$$
\begin{aligned}
&\dot{V} = F_x/m - g\cdot(\cos\alpha\cos\beta\sin\theta - \sin\beta\sin\phi\cos\theta - \sin\alpha\cos\beta\cos\phi\cos\theta),\\
&\dot{h} = V\cdot(\cos\alpha\cos\beta\sin\theta - \sin\beta\sin\phi\cos\theta - \sin\alpha\cos\beta\cos\phi\cos\theta),\\
&\dot{\alpha} = q - (p\cos\alpha + r\sin\alpha)\tan\beta + F_z/(mV\cos\beta) + g/(V\cos\beta)\cdot(\sin\alpha\sin\theta + \cos\alpha\cos\phi\cos\theta),\\
&\dot{q} = -(I_{xx} - I_{zz})/I_{yy}\cdot p\cdot r - I_{xz}/I_{yy}\cdot(p^2 - r^2) + M_y/I_{yy}, \quad \dot{\theta} = q\cos\phi - r\sin\phi,\\
&\dot{\beta} = p\sin\alpha - r\cos\alpha + F_y/(mV) + g/V\cdot(\cos\alpha\sin\beta\sin\theta + \cos\beta\sin\phi\cos\theta - \sin\alpha\sin\beta\cos\phi\cos\theta),\\
&\begin{bmatrix}\dot{p}\\ \dot{r}\end{bmatrix} = \begin{bmatrix} I_{xx} & -I_{xz}\\ -I_{xz} & I_{zz}\end{bmatrix}^{-1}\begin{bmatrix}(I_{yy} - I_{zz})q\cdot r + I_{xz}p\cdot q + M_x\\ (I_{xx} - I_{yy})p\cdot q - I_{xz}q\cdot r + M_z\end{bmatrix},\\
&\dot{\phi} = p + q\sin\phi\tan\theta + r\cos\phi\tan\theta, \quad \dot{\psi} = q\sin\phi/\cos\theta + r\cos\phi/\cos\theta,
\end{aligned}
\tag{1}
$$

where m is the mass, g is the acceleration of gravity, h is the flight height, I_{xx}, I_{yy}, I_{zz}, and I_{xz} are the rotational inertias and product of inertia in the x-z plane.

In (1), $[F_x\ \ F_y\ \ F_z]^\mathrm{T}$ and $[M_x\ \ M_y\ \ M_z]^\mathrm{T}$ are the resultant forces and moments in $O_\mathrm{w}x_\mathrm{w}y_\mathrm{w}z_\mathrm{w}$ and

$O_\mathrm{b}x_\mathrm{b}y_\mathrm{b}z_\mathrm{b}$:

$$\begin{aligned} &F_x = -\mathcal{D} + F_{\mathrm{r}x}, \quad F_y = \mathcal{S} + F_{\mathrm{r}y}, \quad F_z = -\mathcal{L} + F_{\mathrm{r}z}, \\ &M_x = \mathcal{R} + M_{Fx} + M_{Qx}, \quad M_y = \mathcal{P} + M_{Fy}, \quad M_z = \mathcal{Y} + M_{Fz} + M_{Qz}, \end{aligned} \tag{2}$$

where $[\mathcal{D}\ \mathcal{S}\ \mathcal{L}]^\mathrm{T}$ are the aerodynamic drag, side force, and lift, $[\mathcal{R}\ \mathcal{P}\ \mathcal{Y}]^\mathrm{T}$ are the aerodynamic rolling, pitching, and yawing moments. Four rotors with corresponding rotor-tilt angles generate forces $[F_{\mathrm{r}x}\ F_{\mathrm{r}y}\ F_{\mathrm{r}z}]^\mathrm{T}$, moments $[M_{Fx}\ M_{Fy}\ M_{Fz}]^\mathrm{T}$ from thrusts, and moments $[M_{Qx}\ 0\ M_{Qz}]^\mathrm{T}$ from reaction torques.

The aerodynamic forces and moments in (2) are as follows:

$$[\mathcal{D}\ \mathcal{S}\ \mathcal{L}]^\mathrm{T} = 1/2 \cdot \rho V^2 S [C_\mathcal{D}\ C_\mathcal{S}\ C_\mathcal{L}]^\mathrm{T}, \quad [\mathcal{R}\ \mathcal{P}\ \mathcal{Y}]^\mathrm{T} = 1/2 \cdot \rho V^2 S [\bar{b} C_\mathcal{R}\ \bar{c} C_\mathcal{P}\ \bar{b} C_\mathcal{Y}]^\mathrm{T}, \tag{3}$$

where ρ is the air density, S is the wing area, $\bar{b}$ is the wingspan, and $\bar{c}$ is the average wing chord length. The aerodynamic coefficients in (3) are postulated as the following forms:

$$\begin{aligned} &C_\mathcal{D} = C_{\mathcal{D}0} + C_{\mathcal{D}1}\alpha + C_{\mathcal{D}2}\alpha^2, \quad C_\mathcal{S} = C_{\mathcal{S}1}\beta + \bar{b}/(2V) \cdot (C_{\mathcal{S}p}p + C_{\mathcal{S}r}r), \\ &C_\mathcal{L} = C_{\mathcal{L}0} + C_{\mathcal{L}1}\alpha + \bar{c}/(2V) \cdot C_{\mathcal{L}q}q, \quad C_\mathcal{R} = C_{\mathcal{R}1}\beta + \bar{b}/(2V) \cdot (C_{\mathcal{R}p}p + C_{\mathcal{R}r}r), \\ &C_\mathcal{P} = C_{\mathcal{P}0} + C_{\mathcal{P}1}\alpha + \bar{c}/(2V) \cdot C_{\mathcal{P}q}q, \quad C_\mathcal{Y} = C_{\mathcal{Y}1}\beta + \bar{b}/(2V) \cdot (C_{\mathcal{Y}p}p + C_{\mathcal{Y}r}r), \end{aligned} \tag{4}$$

where the parameters in the above right hand sides (RHSs) are all unknown but constant, and the stepwise regression procedure can be applied for the forms of aerodynamic coefficients [10].

For the tiltable rotors shown in Figure 1, generated rotor thrusts and reaction torques are represented as $F_\mathrm{r}(\omega_i)$ and $Q_\mathrm{r}(\omega_i)$, where ω_i $(i = 1, \ldots, 4)$ is the PWM signal of ith rotor. With the rotor-tilt angle signed by i_{ni}, the average rotor-tilt angle $i_n = 1/4 \sum_{i=1}^4 i_{ni} = \pi/2$ rad or 0 rad is defined in helicopter mode or airplane mode. Rotor thrusts should be transformed from $O_\mathrm{b}x_\mathrm{b}y_\mathrm{b}z_\mathrm{b}$ into $O_\mathrm{w}x_\mathrm{w}y_\mathrm{w}z_\mathrm{w}$, and the following forces and moments are formulated for (2):

$$\begin{aligned} &[F_{\mathrm{r}x}\ F_{\mathrm{r}y}\ F_{\mathrm{r}z}]^\mathrm{T} = \sum_{i=1}^4 [\cos(\alpha + i_{ni})\cos\beta F_\mathrm{r}(\omega_i)\ \ -\cos(\alpha + i_{ni})\sin\beta F_\mathrm{r}(\omega_i)\ \ -\sin(\alpha + i_{ni}) F_\mathrm{r}(\omega_i)]^\mathrm{T}, \\ &M_{Fx} = y_\mathrm{rf} \cdot (\sin i_{n1} F_\mathrm{r}(\omega_1) - \sin i_{n2} F_\mathrm{r}(\omega_2)) + y_\mathrm{rb} \cdot (\sin i_{n4} F_\mathrm{r}(\omega_4) - \sin i_{n3} F_\mathrm{r}(\omega_3)), \\ &M_{Fy} = x_\mathrm{rf} \cdot (\sin i_{n1} F_\mathrm{r}(\omega_1) + \sin i_{n2} F_\mathrm{r}(\omega_2)) - x_\mathrm{rb} \cdot (\sin i_{n3} F_\mathrm{r}(\omega_3) + \sin i_{n4} F_\mathrm{r}(\omega_4)), \\ &M_{Fz} = y_\mathrm{rf} \cdot (\cos i_{n1} F_\mathrm{r}(\omega_1) - \cos i_{n2} F_\mathrm{r}(\omega_2)) + y_\mathrm{rb} \cdot (\cos i_{n4} F_\mathrm{r}(\omega_4) - \cos i_{n3} F_\mathrm{r}(\omega_3)), \\ &M_{Qx} = \cos i_{n1} Q_\mathrm{r}(\omega_1) - \cos i_{n2} Q_\mathrm{r}(\omega_2) + \cos i_{n3} Q_\mathrm{r}(\omega_3) - \cos i_{n4} Q_\mathrm{r}(\omega_4), \\ &M_{Qz} = -\sin i_{n1} Q_\mathrm{r}(\omega_1) + \sin i_{n2} Q_\mathrm{r}(\omega_2) - \sin i_{n3} Q_\mathrm{r}(\omega_3) + \sin i_{n4} Q_\mathrm{r}(\omega_4), \end{aligned} \tag{5}$$

where x_rf, x_rb, y_rf, and y_rb are the longitudinal and lateral distances from rotors to COG.

Based on modeling assumptions, (1)–(5) formulate the nominal model of the quad-TRUAV. The integrated nonlinear model of the quad-TRUAV is proposed as follows:

$$\dot{\boldsymbol{x}}(t) = \boldsymbol{f}_\mathrm{c}(\boldsymbol{x}(t), \boldsymbol{u}(t)) + \boldsymbol{E}\boldsymbol{e}_\mathrm{c}(t), \quad \boldsymbol{y}(t) = \boldsymbol{x}(t), \tag{6}$$

where $\dot{\boldsymbol{x}}(t) = \boldsymbol{f}_\mathrm{c}(\boldsymbol{x}(t), \boldsymbol{u}(t))$ is the nominal model, $\boldsymbol{x} = [V\ \alpha\ q\ h\ \theta\ \beta\ p\ r\ \phi\ \psi]^\mathrm{T}$ is the state vector, $\boldsymbol{u} = [i_{n1}\ \cdots\ i_{n4}\ \omega_1\ \cdots\ \omega_4]^\mathrm{T}$ is the control input vector, $\boldsymbol{y}$ is the measurement output vector, $\boldsymbol{e}_\mathrm{c}$ is the defined model error vector to accommodate all model mismatches from modeling assumptions and some other inaccuracy, and $\boldsymbol{E}$ is a parameter matrix. For the nonlinear model identification, the model about rotor-tilt angles can refer to [9] without details. In addition, some unknown parameters in the RHSs of (4) will be estimated, the rotor models $F_\mathrm{r}(\cdot)$ and $Q_\mathrm{r}(\cdot)$ for (5) will be identified, and the model error vector in (6) will also be arranged to further improve the accuracy of the model. To collect flight data for these tasks, Section 3 will introduce the attitude control method for the quad-TRUAV flight experiments.

3 Attitude control method

Without the tilt corridor of the quad-TRUAV for its safe velocity control, this section focuses on the attitude stability mainly. The rotational dynamics in the quad-TRUAV nominal model will be reformulated and simplified as the port-controlled Hamiltonian (PCH) model, and the attitude control with a smooth-switch structure will be designed based on the improved IDA-PBC for flight experiments.

3.1 Rotational dynamics simplification

In the aspect of energy [16], the rotational dynamics in the quad-TRUAV nominal model can be represented as an Euler-Lagrange (EL) equation $\boldsymbol{J}(\boldsymbol{\eta})\ddot{\boldsymbol{\eta}} + \boldsymbol{C}(\boldsymbol{\eta}, \dot{\boldsymbol{\eta}})\dot{\boldsymbol{\eta}} = \boldsymbol{M_u}$, where $\boldsymbol{\eta} = [\phi\ \theta\ \psi]^{\mathrm{T}}$, $\boldsymbol{M_u} = [M_x\ M_y\ M_z]^{\mathrm{T}}$, $\boldsymbol{J}(\boldsymbol{\eta})$ is the inertia matrix, and $\boldsymbol{C}(\boldsymbol{\eta}, \dot{\boldsymbol{\eta}})$ is the Coriolis and centrifugal matrix as $\boldsymbol{C}(\boldsymbol{\eta}, \dot{\boldsymbol{\eta}}) = \dot{\boldsymbol{J}}(\boldsymbol{\eta}) - \frac{1}{2}\frac{\partial \dot{\boldsymbol{\eta}}^{\mathrm{T}} \boldsymbol{J}(\boldsymbol{\eta})}{\partial \boldsymbol{\eta}}$ with $\boldsymbol{J}(\boldsymbol{\eta}) = \boldsymbol{R}_{\boldsymbol{\eta}}^{\mathrm{T}} \boldsymbol{\mathcal{J}} \boldsymbol{R}_{\boldsymbol{\eta}}$,

$$\boldsymbol{\mathcal{J}} = \begin{bmatrix} I_{xx} & 0 & -I_{xz} \\ 0 & I_{yy} & 0 \\ -I_{xz} & 0 & I_{zz} \end{bmatrix}, \quad \boldsymbol{R}_{\boldsymbol{\eta}} = \begin{bmatrix} 1 & 0 & -\sin\theta \\ 0 & \cos\phi & \sin\phi\cos\theta \\ 0 & -\sin\phi & \cos\phi\cos\theta \end{bmatrix}.$$

By defining a Hamiltonian $\mathcal{H}(\boldsymbol{\eta}, \boldsymbol{\kappa}) = 1/2 \cdot \boldsymbol{\kappa}^{\mathrm{T}} \boldsymbol{J}^{-1}(\boldsymbol{\eta})\boldsymbol{\kappa}$ as the total energy of rotational dynamics with the angular momentum $\boldsymbol{\kappa} = \boldsymbol{J}(\boldsymbol{\eta})\dot{\boldsymbol{\eta}}$, the above EL equation is equivalent to the following PCH model:

$$\begin{bmatrix} \dot{\boldsymbol{\eta}} \\ \dot{\boldsymbol{\kappa}} \end{bmatrix} = \begin{bmatrix} \boldsymbol{0} & \boldsymbol{I}_n \\ -\boldsymbol{I}_n & \boldsymbol{0} \end{bmatrix} \begin{bmatrix} \nabla_{\boldsymbol{\eta}}\mathcal{H} \\ \nabla_{\boldsymbol{\kappa}}\mathcal{H} \end{bmatrix} + \begin{bmatrix} \boldsymbol{0} \\ \boldsymbol{I}_n \end{bmatrix} \boldsymbol{M_u}, \tag{7}$$

where $\nabla_{\boldsymbol{\kappa}}\mathcal{H} = \boldsymbol{J}^{-1}(\boldsymbol{\eta})\boldsymbol{\kappa}$, $\nabla_{\boldsymbol{\eta}}\mathcal{H} = -\frac{1}{2}\frac{\partial \dot{\boldsymbol{\eta}}^{\mathrm{T}} \boldsymbol{J}(\boldsymbol{\eta})}{\partial \boldsymbol{\eta}}\dot{\boldsymbol{\eta}}$, and $\boldsymbol{I}_n$ is an identity matrix with $n = 3$.

According to (5), the applied control inputs in $\boldsymbol{u} = [i_{n1}\ \cdots\ i_{n4}\ \omega_1\ \cdots\ \omega_4]^{\mathrm{T}}$ affect rotor thrusts and generate the main effects for the attitude control. To reformulate the format of $\boldsymbol{M_u}$, some virtual control inputs i_n, Δi_{nq}, Δi_{pr}, F_{r}, $\Delta F_{\mathrm{r}q}$, and ΔF_{pr} that satisfy the following equations are defined:

$$\begin{aligned} &i_{n1} = i_n + \Delta i_{nq} + \Delta i_{pr},\ i_{n2} = i_n + \Delta i_{nq} - \Delta i_{pr},\ i_{n3} = i_n - \Delta i_{nq} - \Delta i_{pr},\ i_{n4} = i_n - \Delta i_{nq} + \Delta i_{pr}, \\ &F_{\mathrm{r}1} = F_{\mathrm{r}}(\omega_1) = x_{\mathrm{r}}/x_{\mathrm{rf}} \cdot (F_{\mathrm{r}} + \Delta F_{\mathrm{r}q} + \Delta F_{pr}),\ F_{\mathrm{r}2} = F_{\mathrm{r}}(\omega_2) = x_{\mathrm{r}}/x_{\mathrm{rf}} \cdot (F_{\mathrm{r}} + \Delta F_{\mathrm{r}q} - \Delta F_{pr}), \\ &F_{\mathrm{r}3} = F_{\mathrm{r}}(\omega_3) = x_{\mathrm{r}}/x_{\mathrm{rb}} \cdot (F_{\mathrm{r}} - \Delta F_{\mathrm{r}q} - \Delta F_{pr}),\ F_{\mathrm{r}4} = F_{\mathrm{r}}(\omega_4) = x_{\mathrm{r}}/x_{\mathrm{rb}} \cdot (F_{\mathrm{r}} - \Delta F_{\mathrm{r}q} + \Delta F_{pr}), \end{aligned} \tag{8}$$

where i_n is the average rotor-tilt angle, Δi_{nq} is the difference between forward and backward rotor-tilt angles, Δi_{pr} is the difference between left and right rotor-tilt angles, F_{r} is the average rotor thrust, $\Delta F_{\mathrm{r}q}$ is the difference between forward and backward rotor thrusts, ΔF_{pr} is the difference between left and right rotor thrusts, and constants x_{r} and y_{r} satisfy $y_{\mathrm{r}}/x_{\mathrm{r}} = 1/2(y_{\mathrm{rf}}/x_{\mathrm{rf}} + y_{\mathrm{rb}}/x_{\mathrm{rb}})$. By introducing (8) into M_{Fx}, M_{Fy}, and M_{Fz} in (5), the trigonometric functions therein can be extended with respect to i_n, Δi_{nq}, and Δi_{pr}, and further multiplied by the rotor thrusts about F_{r}, $\Delta F_{\mathrm{r}q}$, and ΔF_{pr}. Thus moments M_{Fx}, M_{Fy}, and M_{Fz} can be extended as the forms related to the above virtual control inputs. Because some virtual values are always small, the following approximations are considered:

$$\cos\Delta i_{nq} \approx 1,\ \cos\Delta i_{pr} \approx 1,\ \sin\Delta i_{nq}\sin\Delta i_{pr} \approx 0,\ \sin\Delta i_{nq}\Delta F_{pr} \approx 0,\ \sin\Delta i_{pr}\Delta F_{\mathrm{r}q} \approx 0, \tag{9}$$

and then the moments in (2) are reformulated as follows:

$$\boldsymbol{M_u} = \begin{bmatrix} M_x \\ M_y \\ M_z \end{bmatrix} = \begin{bmatrix} M_{Fx} + M_{Qx} + \mathcal{R} \\ M_{Fy} + \mathcal{P} \\ M_{Fz} + M_{Qz} + \mathcal{Y} \end{bmatrix} = \begin{bmatrix} 4y_{\mathrm{r}}(\sin i_n \cdot \Delta F_{pr} + \cos i_n \cdot F_{\mathrm{r}}\sin\Delta i_{pr}) + \tilde{d}_\phi + M_{Qx} + \mathcal{R} \\ 4x_{\mathrm{r}}(\sin i_n \cdot \Delta F_{\mathrm{r}q} + \cos i_n \cdot F_{\mathrm{r}}\sin\Delta i_{nq}) + \tilde{d}_\theta + \mathcal{P} \\ 4y_{\mathrm{r}}(\cos i_n \cdot \Delta F_{pr} - \sin i_n \cdot F_{\mathrm{r}}\sin\Delta i_{pr}) + \tilde{d}_\psi + M_{Qz} + \mathcal{Y} \end{bmatrix}, \tag{10}$$

where the forms of M_{Fx}, M_{Fy}, and M_{Fz} are simplified based on (9), the virtual control inputs that take main control effects are reserved, and some items are ignored directly because they are additional from the dynamic coupling. Three variables $\tilde{d}_\phi$, $\tilde{d}_\theta$, and $\tilde{d}_\psi$ are introduced to consider the simplification errors from the above ignored items.

For the virtual control inputs ΔF_{pr}, Δi_{pr}, $\Delta F_{\mathrm{r}q}$, and Δi_{nq} in (10), the following forms are proposed:

$$\begin{aligned} &\Delta F_{pr} = \sin i_n \cdot \mathcal{C}_{\mathrm{H}p} + \cos i_n \cdot \mathcal{C}_{\mathrm{A}r},\quad \Delta i_{pr} \approx \sin\Delta i_{pr} = -\sin i_n \cdot \mathcal{C}_{\mathrm{H}r} + \cos i_n \cdot \mathcal{C}_{\mathrm{A}p}, \\ &\Delta F_{\mathrm{r}q} = \sin i_n \cdot \mathcal{C}_{\mathrm{H}q},\quad \Delta i_{nq} \approx \sin\Delta i_{nq} = \cos i_n \cdot \mathcal{C}_{\mathrm{A}q}, \end{aligned} \tag{11}$$

and Eq. (10) is equivalent as follows:

$$\boldsymbol{M}_{\boldsymbol{u}} = \sin^2 i_n \cdot \boldsymbol{B}_{\rm H}\boldsymbol{u}_{\rm H} + \cos^2 i_n \cdot \boldsymbol{B}_{\rm A}\boldsymbol{u}_{\rm A} + \overline{\boldsymbol{d}} + \boldsymbol{d}, \tag{12}$$

where

$$\boldsymbol{B}_{\rm H} = \begin{bmatrix} 4y_{\rm r} & 0 & 0 \\ 0 & 4x_{\rm r} & 0 \\ 0 & 0 & 4y_{\rm r}F_{\rm r} \end{bmatrix}, \quad \boldsymbol{u}_{\rm H} = \begin{bmatrix} \mathcal{C}_{{\rm H}p} \\ \mathcal{C}_{{\rm H}q} \\ \mathcal{C}_{{\rm H}r} \end{bmatrix}, \quad \boldsymbol{B}_{\rm A} = \begin{bmatrix} 4y_{\rm r}F_{\rm r} & 0 & 0 \\ 0 & 4x_{\rm r}F_{\rm r} & 0 \\ 0 & 0 & 4y_{\rm r} \end{bmatrix}, \quad \boldsymbol{u}_{\rm A} = \begin{bmatrix} \mathcal{C}_{{\rm A}p} \\ \mathcal{C}_{{\rm A}q} \\ \mathcal{C}_{{\rm A}r} \end{bmatrix},$$

and $\overline{\boldsymbol{d}}+\boldsymbol{d} = [4y_{\rm r}\sin i_n \cos i_n(\mathcal{C}_{{\rm A}r} - F_{\rm r}\mathcal{C}_{{\rm H}r}) + M_{Qx} + \mathcal{R} + \tilde{d}_\phi \ \mathcal{P} + \tilde{d}_\theta \ 4y_{\rm r}\sin i_n \cos i_n(\mathcal{C}_{{\rm H}p} - F_{\rm r}\mathcal{C}_{{\rm A}p}) + M_{Qz} + \mathcal{Y} + \tilde{d}_\psi]^{\rm T}$. In the above equation, $\overline{\boldsymbol{d}}$ and $\boldsymbol{d}$ are defined and reformulate all simplifications as two disturbance vectors to facilitate the following control design, where $\overline{\boldsymbol{d}}$ is large-sized but slowly varying ($\dot{\overline{\boldsymbol{d}}} \approx \boldsymbol{0}$), and $\boldsymbol{d}$ is small-sized and time-varying. Vectors $\boldsymbol{u}_{\rm H} = [\mathcal{C}_{{\rm H}p} \ \mathcal{C}_{{\rm H}q} \ \mathcal{C}_{{\rm H}r}]^{\rm T}$ and $\boldsymbol{u}_{\rm A} = [\mathcal{C}_{{\rm A}p} \ \mathcal{C}_{{\rm A}q} \ \mathcal{C}_{{\rm A}r}]^{\rm T}$ can be regarded as virtual control inputs for Helicopter mode ($i_n = \pi/2$ rad) and Airplane mode ($i_n = 0$ rad). Consequently, the PCH model of the quad-TRUAV rotational dynamics (7) is reformulated as follows:

$$\begin{bmatrix} \dot{\boldsymbol{\eta}} \\ \dot{\boldsymbol{\kappa}} \end{bmatrix} = \begin{bmatrix} \boldsymbol{0} & \boldsymbol{I}_n \\ -\boldsymbol{I}_n & \boldsymbol{0} \end{bmatrix} \begin{bmatrix} \nabla_{\boldsymbol{\eta}}\mathcal{H} \\ \nabla_{\boldsymbol{\kappa}}\mathcal{H} \end{bmatrix} + \sin^2 i_n \begin{bmatrix} \boldsymbol{0} \\ \boldsymbol{B}_{\rm H} \end{bmatrix} \boldsymbol{u}_{\rm H} + \cos^2 i_n \begin{bmatrix} \boldsymbol{0} \\ \boldsymbol{B}_{\rm A} \end{bmatrix} \boldsymbol{u}_{\rm A} + \begin{bmatrix} \boldsymbol{0} \\ \overline{\boldsymbol{d}} \end{bmatrix} + \begin{bmatrix} \boldsymbol{0} \\ \boldsymbol{d} \end{bmatrix}, \tag{13}$$

which is a parameter-dependent PCH model with respect to $\sin^2 i_n$ and $\cos^2 i_n$.

This subsection simplifies the rotational dynamics of the quad-TRUAV as the PCH model (13), where new virtual control inputs $\boldsymbol{u}_{\rm H} = [\mathcal{C}_{{\rm H}p} \ \mathcal{C}_{{\rm H}q} \ \mathcal{C}_{{\rm H}r}]^{\rm T}$ and $\boldsymbol{u}_{\rm A} = [\mathcal{C}_{{\rm A}p} \ \mathcal{C}_{{\rm A}q} \ \mathcal{C}_{{\rm A}r}]^{\rm T}$ are introduced. Based on (11), $\boldsymbol{u}_{\rm H}$ and $\boldsymbol{u}_{\rm A}$ can be transformed into the original virtual control inputs, and (11) implies the smooth-switch structure dependent on the average rotor-tilt angle i_n for the TRUAV attitude control.

3.2 Attitude control via IDA-PBC

With the parameter-dependent PCH model (13) as the controlled plant, the slowly varying disturbance vector $\overline{\boldsymbol{d}}$ in the model should be compensated, and the stability under the time-varying disturbance vector $\boldsymbol{d}$ should be analyzed. For these purposes, the improved IDA-PBC with the integral action and some fundamental knowledge about passivity will be applied in this subsection [16, 17, 27].

To compensate some disturbances by the integral action, a state transformation is necessary [17]:

$$\boldsymbol{z}_{\boldsymbol{\eta}} = \boldsymbol{\eta}, \quad \boldsymbol{z}_{\boldsymbol{\kappa}} = \boldsymbol{\kappa} + k_{\boldsymbol{\eta}}\nabla_{\boldsymbol{z}_{\boldsymbol{\eta}}}\mathcal{H}_{\rm d} \tag{14}$$

with the desired Hamiltonian:

$$\mathcal{H}_{\rm d}(\boldsymbol{z}_{\boldsymbol{\eta}}, \boldsymbol{z}_{\boldsymbol{\kappa}}, \boldsymbol{z}_{\rm i}) = 1/2 \cdot \boldsymbol{z}_{\boldsymbol{\kappa}}^{\rm T}\boldsymbol{J}_{\rm d}^{-1}(\boldsymbol{\eta})\boldsymbol{z}_{\boldsymbol{\kappa}} + \mathcal{V}_{\rm d}(\boldsymbol{\eta}) + 1/2 \cdot (\boldsymbol{z}_{\rm i} - \overline{\boldsymbol{d}})^{\rm T}\boldsymbol{K}_{\rm i}^{-1}(\boldsymbol{z}_{\rm i} - \overline{\boldsymbol{d}}), \tag{15}$$

where $\boldsymbol{J}_{\rm d}(\boldsymbol{\eta}) > 0$, $k_{\boldsymbol{\eta}} > 0$ is a scalar, $\boldsymbol{K}_{\rm i} > 0$, $\boldsymbol{z}_{\rm i}$ is an auxiliary vector for the integral action, and $\mathcal{V}_{\rm d}(\boldsymbol{\eta})$ should satisfy the following condition for the tracking towards a constant reference $\boldsymbol{\eta}_{\rm d}$:

$$\boldsymbol{\eta}_{\rm d} = \arg\min \mathcal{H}_{\rm d}(\boldsymbol{z}_{\boldsymbol{\eta}}, \boldsymbol{z}_{\boldsymbol{\kappa}}, \boldsymbol{z}_{\rm i}) = \arg\min \mathcal{V}_{\rm d}(\boldsymbol{\eta}) \text{ i.e., } \nabla_{\boldsymbol{z}_{\boldsymbol{\eta}}}\mathcal{V}_{\rm d}(\boldsymbol{\eta}_{\rm d}) = 0, \ \nabla^2_{\boldsymbol{z}_{\boldsymbol{\eta}}}\mathcal{V}_{\rm d}(\boldsymbol{\eta}_{\rm d}) > 0. \tag{16}$$

Two sets of control inputs for helicopter and airplane modes are designed as the following form:

$$\boldsymbol{B}_\star\boldsymbol{u}_\star = -\boldsymbol{K}_{{\rm d}\star}\boldsymbol{J}_{\rm d}^{-1}(\boldsymbol{\eta})\boldsymbol{\kappa} - k_{\boldsymbol{\eta}}(\nabla_{\boldsymbol{z}_{\boldsymbol{\eta}}}\mathcal{H}_{\rm d})' - \boldsymbol{z}_{\rm i} + \nabla_{\boldsymbol{\eta}}\mathcal{H} - [\boldsymbol{K}_{{\rm d}\star}\boldsymbol{J}_{\rm d}^{-1}(\boldsymbol{\eta})k_{\boldsymbol{\eta}} + \boldsymbol{J}_{\rm d}(\boldsymbol{\eta})\boldsymbol{J}^{-1}(\boldsymbol{\eta})]\nabla_{\boldsymbol{z}_{\boldsymbol{\eta}}}\mathcal{H}_{\rm d}, \tag{17}$$

where $\star = $ H or A for different flight modes and $\boldsymbol{K}_{{\rm d}\star} > 0$. By introducing (17) into (13), the closed-loop system is formulated as follows with $\boldsymbol{K}_{\rm d}(i_n) = \sin^2 i_n\boldsymbol{K}_{\rm dH} + \cos^2 i_n\boldsymbol{K}_{\rm dA}$:

$$\begin{bmatrix} \dot{\boldsymbol{z}}_{\boldsymbol{\eta}} \\ \dot{\boldsymbol{z}}_{\boldsymbol{\kappa}} \\ \dot{\boldsymbol{z}}_{\rm i} \end{bmatrix} = \begin{bmatrix} -k_{\boldsymbol{\eta}}\boldsymbol{J}^{-1}(\boldsymbol{\eta}) & \boldsymbol{J}^{-1}(\boldsymbol{\eta})\boldsymbol{J}_{\rm d}(\boldsymbol{\eta}) & \boldsymbol{0} \\ -\boldsymbol{J}_{\rm d}(\boldsymbol{\eta})\boldsymbol{J}^{-1}(\boldsymbol{\eta}) & -\boldsymbol{K}_{\rm d}(i_n) & -\boldsymbol{K}_{\rm i} \\ \boldsymbol{0} & \boldsymbol{K}_{\rm i} & \boldsymbol{0} \end{bmatrix} \begin{bmatrix} \nabla_{\boldsymbol{z}_{\boldsymbol{\eta}}}\mathcal{H}_{\rm d} \\ \nabla_{\boldsymbol{z}_{\boldsymbol{\kappa}}}\mathcal{H}_{\rm d} \\ \nabla_{\boldsymbol{z}_{\rm i}}\mathcal{H}_{\rm d} \end{bmatrix} + \begin{bmatrix} \boldsymbol{0} \\ \boldsymbol{d} \\ \boldsymbol{0} \end{bmatrix}. \tag{18}$$

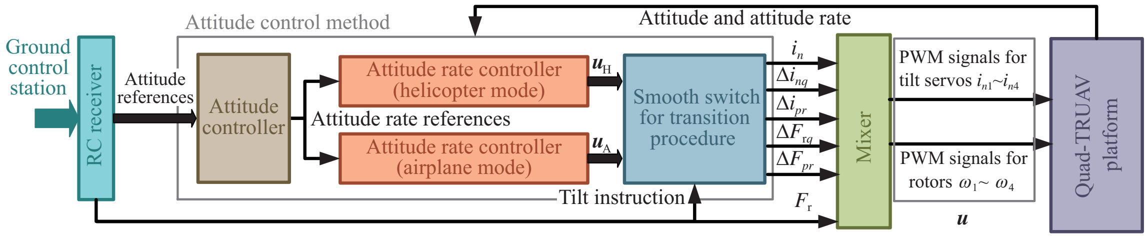

Figure 3 (Color online) Attitude control structure of quad-TRUAV.

Theorem 1 will analyze the stability of this closed-loop system.

Theorem 1. With the control input vector in (17), the closed-loop system (18) of the controlled plant (13) can be formulated. If $\boldsymbol{d} = \boldsymbol{0}$, the asymptotic stability of $\nabla_{\boldsymbol{z}_{\boldsymbol{\eta}}}\mathcal{H}_{\rm d}$ and $\nabla_{\boldsymbol{z}_{\boldsymbol{\kappa}}}\mathcal{H}_{\rm d}$ will be achieved with the slowly varying i_n, i.e., $\lim_{t\to+\infty} \nabla_{\boldsymbol{z}_{\boldsymbol{\eta}}}\mathcal{H}_{\rm d} = \lim_{t\to+\infty} \nabla_{\boldsymbol{\eta}}\mathcal{H}_{\rm d} = \boldsymbol{0}$, $\lim_{t\to+\infty} \nabla_{\boldsymbol{z}_{\boldsymbol{\kappa}}}\mathcal{H}_{\rm d} = \lim_{t\to+\infty} \boldsymbol{J}_{\rm d}^{-1}(\boldsymbol{\eta})\boldsymbol{z}_{\boldsymbol{\kappa}} = \boldsymbol{0}$, and $\lim_{t\to+\infty} \boldsymbol{z}_{\boldsymbol{\kappa}} = \boldsymbol{0}$; if $\boldsymbol{d} \neq \boldsymbol{0}$, the $\mathcal{L}_2$ stability of $\boldsymbol{d} \mapsto \nabla_{\boldsymbol{z}_{\boldsymbol{\kappa}}}\mathcal{H}_{\rm d}$ will be satisfied.

Proof. By regarding (15) as the Lyapunov function, its derivative against time is as follows:

$$\begin{aligned}\dot{\mathcal{H}}_{\rm d} &= [\nabla^{\rm T}_{\boldsymbol{z}_{\boldsymbol{\eta}}}\mathcal{H}_{\rm d}\ \nabla^{\rm T}_{\boldsymbol{z}_{\boldsymbol{\kappa}}}\mathcal{H}_{\rm d}\ \nabla^{\rm T}_{\boldsymbol{z}_{\rm i}}\mathcal{H}_{\rm d}][\dot{\boldsymbol{z}}^{\rm T}_{\boldsymbol{\eta}}\ \dot{\boldsymbol{z}}^{\rm T}_{\boldsymbol{\kappa}}\ \dot{\boldsymbol{z}}^{\rm T}_{\rm i}]^{\rm T}\\ &= -\nabla_{\boldsymbol{z}_{\boldsymbol{\eta}}}\mathcal{H}^{\rm T}_{\rm d}\cdot k_{\boldsymbol{\eta}}\boldsymbol{J}^{-1}(\boldsymbol{\eta})\nabla_{\boldsymbol{z}_{\boldsymbol{\eta}}}\mathcal{H}_{\rm d} - \nabla_{\boldsymbol{z}_{\boldsymbol{\kappa}}}\mathcal{H}^{\rm T}_{\rm d}\boldsymbol{K}_{\rm d}(i_n)\nabla_{\boldsymbol{z}_{\boldsymbol{\kappa}}}\mathcal{H}_{\rm d} + \nabla_{\boldsymbol{z}_{\boldsymbol{\kappa}}}\mathcal{H}^{\rm T}_{\rm d}\boldsymbol{d},\end{aligned} \tag{19}$$

where $k_{\boldsymbol{\eta}}\boldsymbol{J}^{-1}(\boldsymbol{\eta}) > 0$ and $\boldsymbol{K}_{\rm d}(i_n) = \sin^2 i_n\boldsymbol{K}_{\rm dH} + \cos^2 i_n\boldsymbol{K}_{\rm dA} > 0$.

If there is no time-varying disturbance, i.e., $\boldsymbol{d} = \boldsymbol{0}$, the derivative of $\mathcal{H}_{\rm d}$ will be in the following form:

$$\dot{\mathcal{H}}_{\rm d} = -\nabla_{\boldsymbol{z}_{\boldsymbol{\eta}}}\mathcal{H}^{\rm T}_{\rm d}\cdot k_{\boldsymbol{\eta}}\boldsymbol{J}^{-1}(\boldsymbol{\eta})\nabla_{\boldsymbol{z}_{\boldsymbol{\eta}}}\mathcal{H}_{\rm d} - \nabla_{\boldsymbol{z}_{\boldsymbol{\kappa}}}\mathcal{H}^{\rm T}_{\rm d}\boldsymbol{K}_{\rm d}(i_n)\nabla_{\boldsymbol{z}_{\boldsymbol{\kappa}}}\mathcal{H}_{\rm d} \leqslant 0. \tag{20}$$

According to the invariant principle [27], the closed-loop system with the slowly varying i_n ($\dot{i}_n \approx 0$) converges to the largest invariant set with $\dot{\mathcal{H}}_{\rm d} = 0$, which means $\nabla_{\boldsymbol{z}_{\boldsymbol{\eta}}}\mathcal{H}_{\rm d} = \boldsymbol{0}$ and $\nabla_{\boldsymbol{z}_{\boldsymbol{\kappa}}}\mathcal{H}_{\rm d} = \boldsymbol{0}$. Because matrix $\boldsymbol{J}_{\rm d}(\boldsymbol{\eta})$ is invertible, $\nabla_{\boldsymbol{z}_{\boldsymbol{\kappa}}}\mathcal{H}_{\rm d} = \boldsymbol{J}_{\rm d}^{-1}(\boldsymbol{\eta})\boldsymbol{z}_{\boldsymbol{\kappa}} = \boldsymbol{0}$ further results in $\boldsymbol{z}_{\boldsymbol{\kappa}} = \boldsymbol{0}$.

If there are some time-varying disturbances, i.e., $\boldsymbol{d} \neq \boldsymbol{0}$, the derivative of $\mathcal{H}_{\rm d}$ will be as follows:

$$\dot{\mathcal{H}}_{\rm d} \leqslant -\nabla_{\boldsymbol{z}_{\boldsymbol{\kappa}}}\mathcal{H}^{\rm T}_{\rm d}\boldsymbol{K}_{\rm d}(i_n)\nabla_{\boldsymbol{z}_{\boldsymbol{\kappa}}}\mathcal{H}_{\rm d} + \nabla_{\boldsymbol{z}_{\boldsymbol{\kappa}}}\mathcal{H}^{\rm T}_{\rm d}\boldsymbol{d}. \tag{21}$$

With the definition about passivity [16], the above equation means $\boldsymbol{d} \mapsto \nabla_{\boldsymbol{z}_{\boldsymbol{\kappa}}}\mathcal{H}_{\rm d}$ is output strictly passive (OSP). Because the OSP property is the sufficient condition of $\mathcal{L}_2$ stability [27], the $\mathcal{L}_2$ stability of $\boldsymbol{d} \mapsto \nabla_{\boldsymbol{z}_{\boldsymbol{\kappa}}}\mathcal{H}_{\rm d}$ is also established.

In the above proof, the slowly varying assumptions $\dot{i}_n \approx 0$ and $\dot{\boldsymbol{\eta}}_{\rm d} \approx 0$ are necessary for the stability analysis of (18), and some new ideas are required to break these assumptions. To further satisfy condition (16), $\mathcal{V}_{\rm d}(\boldsymbol{\eta}) = 1/2\cdot(\boldsymbol{\eta}-\boldsymbol{\eta}_{\rm d})^{\rm T}\boldsymbol{K}_{\rm p}\ (\boldsymbol{\eta}-\boldsymbol{\eta}_{\rm d})$ is defined with $\boldsymbol{K}_{\rm p} > 0$. Because the values of ϕ and θ are all small in normal flight experiments, let $\boldsymbol{J}_{\rm d}(\boldsymbol{\eta}) = \boldsymbol{J}(\boldsymbol{\eta}) \approx \boldsymbol{\mathcal{J}}$ in controller synthesis. Consequently, the simplified format of (17) can be obtained as follows with $\boldsymbol{K}_{\rm p} = k_{\boldsymbol{\eta}}^{-1}\cdot k_{\boldsymbol{\eta}}^{-1}\boldsymbol{\mathcal{J}}$ and $\boldsymbol{\mathcal{K}} = \boldsymbol{\mathcal{J}}^{-1}k_{\boldsymbol{\eta}}\boldsymbol{K}_{\rm p}$:

$$\boldsymbol{u}_\star = \boldsymbol{B}_\star^{-1}(\boldsymbol{K}_{\rm d\star} + \boldsymbol{\mathcal{J}}\boldsymbol{\mathcal{K}})[\boldsymbol{\mathcal{K}}\cdot(\boldsymbol{\eta}_{\rm d}-\boldsymbol{\eta}) - \dot{\boldsymbol{\eta}}] + \boldsymbol{B}_\star^{-1}\boldsymbol{K}_{\rm i}\int_0^t[\boldsymbol{\mathcal{K}}\cdot(\boldsymbol{\eta}_{\rm d}-\boldsymbol{\eta}) - \dot{\boldsymbol{\eta}}]{\rm d}t. \tag{22}$$

By regarding $\boldsymbol{B}_\star^{-1}(\boldsymbol{K}_{\rm d\star} + \boldsymbol{\mathcal{J}}\boldsymbol{\mathcal{K}})$, $\boldsymbol{\mathcal{K}}$, and $\boldsymbol{B}_\star^{-1}\boldsymbol{K}_{\rm i}$ as control parameters directly, the above equation is equivalent to two sets of hierarchical proportional-integral control laws for helicopter and airplane modes.

Based on (11) and (22), the attitude control structure for all flight modes of the quad-TRUAV is displayed in Figure 3, and this kind of hierarchical control structures are popular in real applications [28]. The common attitude controller block is the outer loop to generate the attitude rate references and corresponds to $\boldsymbol{\mathcal{K}}\cdot(\boldsymbol{\eta}_{\rm d}-\boldsymbol{\eta})$ in (22). The attitude rate controller blocks are the inner loop to generate the control input vectors $\boldsymbol{u}_{\rm H}$ and $\boldsymbol{u}_{\rm A}$, which ensure the attitude stability of helicopter mode ($i_n = \pi/2$ rad) and airplane mode ($i_n = 0$ rad), respectively. To transform flight modes automatically in real applications of the designed control structure, an effective transition strategy is applied as [29]: the average rotor-tilt angle i_n would tilt as a fixed value first for acceleration or deceleration; then the quad-TRUAV would tilt into the target mode directly, when the flight velocity is larger or smaller than a threshold value. For the attitude stability in this transition procedure, control inputs $\boldsymbol{u}_{\rm H} = [\mathcal{C}_{{\rm H}p}\ \mathcal{C}_{{\rm H}q}\ \mathcal{C}_{{\rm H}r}]^{\rm T}$ and

$\boldsymbol{u}_{\mathrm{A}} = [\mathcal{C}_{\mathrm{A}p}\ \mathcal{C}_{\mathrm{A}q}\ \mathcal{C}_{\mathrm{A}r}]^{\mathrm{T}}$ need to be switched smoothly according to (11), and the value of i_n for this smooth switch is set by the applied transition strategy. The mixer block in Figure 3 is based on (8) with an inherent thread of Pixhawk to export applied control inputs with PWM forms for tilt servos and ESCs. The flight control code based on Figure 3 is open and presented in website1).

This section designs the attitude control method for quad-TRUAV flight experiments. Because this control method is based on the nominal model format of the quad-TRUAV rather than accurate dynamics, its control performance under unknown model errors might be poor, and the control parameter tuning is usually necessary. To provide the model basis for further control performance improvement, Section 4 will focus on the nonlinear model identification of the quad-TRUAV.

4 Active model-based nonlinear system identification

According to existing references [20–23], the active model-based system identification for a real system consists in two steps: First, by ignoring some unstructured nonlinearities, the nominal model needs to be identified offline to describe the dynamics approximately. Second, model errors need to be defined and estimated online to accommodate all model mismatches between the nominal model and real system. For the quad-TRUAV, this section will identify the nominal model (1)–(5) by the ground and flight tests. Owing to the nonlinearity of the identified nominal model, UKF will be applied to estimate model errors online. For the application of UKF, this section represents the quad-TRUAV model as the following discrete-time form with k and T as the sampling number and period in experiments:

$$\boldsymbol{x}_{k+1} = \boldsymbol{f}(\boldsymbol{x}_k, \boldsymbol{u}_k) + \boldsymbol{E}\boldsymbol{e}_k, \quad \boldsymbol{y}_k = \boldsymbol{x}_k, \tag{23}$$

where $\boldsymbol{x}_{k+1} = \boldsymbol{f}(\boldsymbol{x}_k, \boldsymbol{u}_k)$ is the discrete-time nominal model of the quad-TRUAV, $\boldsymbol{e}_k$ is the discrete-time model error vector, $\boldsymbol{x}_k = \boldsymbol{x}(kT)$, $\boldsymbol{u}_k = \boldsymbol{u}(kT)$, and $\boldsymbol{y}_k = \boldsymbol{y}(kT)$.

4.1 Nominal model identification

4.1.1 *Ground test*

According to the form of the nominal model (1)–(5), the rotor thrust model $F_{\mathrm{r}}(\cdot)$ and reaction torque model $Q_{\mathrm{r}}(\cdot)$ need to be identified, and the ground test aims at this task.

The rotor of the quad-TRUAV is driven by the DC brushless motor, so the generated thrust and reaction torque are formulated as $F_{\mathrm{r}} = K_F\Omega^2$ and $Q_{\mathrm{r}} = K_Q\Omega^2 = K \cdot F_{\mathrm{r}}$ [30], where Ω is the rotor speed, K_F and K_Q are constant parameters, and $K = K_Q/K_F$. Because the rotor speed Ω is regulated by the ESC with the PWM signal ω, it is feasible to map the PWM signal to the rotor thrust and reaction torque directly as $F_{\mathrm{r}}(\omega)$ and $Q_{\mathrm{r}}(\omega)$, and the relationship between ω and Ω can be formulated as a third-order transfer function [31]. Consequently, it is valid to formulate the following transfer functions:

$$\frac{\overline{F}_{\mathrm{r}}(z)}{\overline{\omega}(z)} = \sqrt{K_F}\frac{\Omega(z)}{\overline{\omega}(z)} = \frac{b_3z^3 + b_2z^2 + b_1z + b_0}{z^3 + a_2z^2 + a_1z + a_0}, \quad \frac{\overline{Q}_{\mathrm{r}}(z)}{\overline{\omega}(z)} = \sqrt{K}\frac{\overline{F}_{\mathrm{r}}(z)}{\overline{\omega}(z)} = \overline{K}\frac{b_3z^3 + b_2z^2 + b_1z + b_0}{z^3 + a_2z^2 + a_1z + a_0}, \tag{24}$$

where $\overline{F}_{\mathrm{r}}(z)$, $\overline{Q}_{\mathrm{r}}(z)$, and $\overline{\omega}(z)$ are the z-transformations of time-domain signals $\overline{F}_{\mathrm{r}} = \sqrt{F_{\mathrm{r}}}$, $\overline{Q}_{\mathrm{r}} = \sqrt{Q_{\mathrm{r}}}$, and $\overline{\omega} = \omega - \omega_0$, ω_0 is the initial value of the PWM signal, and $\overline{K} = \sqrt{K}$.

To estimate unknown a_{i_a} ($i_a = 0, \ldots, 2$), b_{i_b} ($i_b = 0, \ldots, 3$), and $\overline{K}$ in (24), the rotor thrust and reaction torque should be measured. For this purpose, the platform shown in Figure 4 is constructed for the ground test, where the six-dimension force sensor can measure the force and moment in the vertical direction. Together with the recorded PWM signals corresponding to the measured forces and moments, Eq. (24) can be transformed as the following autoregressive exogenous (ARX) models:

$$\begin{aligned}
&\overline{F}_{\mathrm{r}}(kT) + a_2\overline{F}_{\mathrm{r}}((k-1)T) + a_1\overline{F}_{\mathrm{r}}((k-2)T) + a_0\overline{F}_{\mathrm{r}}((k-3)T) \\
&= b_3\overline{\omega}(kT) + b_2\overline{\omega}((k-1)T) + b_1\overline{\omega}((k-2)T) + b_0\overline{\omega}((k-3)T), \\
&\overline{K} \cdot \overline{F}_{\mathrm{r}}(kT) = \overline{Q}_{\mathrm{r}}(kT).
\end{aligned} \tag{25}$$

1) https://github.com/LiuZhongSIA/px4_vtol/tree/V44.

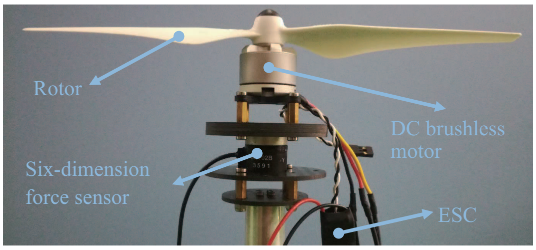

Figure 4 (Color online) Ground test platform.

Figure 5 (Color online) Cruise flight experiment.

By considering the measured values and recorded PWM signals in N sampling periods, the following equations can be formulated for the parameter estimation:

$$\boldsymbol{A}_F\boldsymbol{c}_F = \boldsymbol{b}_F, \quad \boldsymbol{A}_Q\boldsymbol{c}_Q = \boldsymbol{b}_Q, \tag{26}$$

where $\boldsymbol{A}_F \in \mathbb{R}^{(N-3)\times 7}$, $\boldsymbol{b}_F = [\overline{F}_{\rm r}(4T)\ \cdots\ \overline{F}_{\rm r}(NT)]^{\rm T}$, $\boldsymbol{A}_Q \in \mathbb{R}^N$, and $\boldsymbol{b}_Q = [\overline{Q}_{\rm r}(T)\ \cdots\ \overline{Q}_{\rm r}(NT)]^{\rm T}$. Unknown $\boldsymbol{c}_F = [a_2\ a_1\ a_0\ b_3\ b_2\ b_1\ b_0]^{\rm T}$ and $\boldsymbol{c}_Q = \overline{K}$ include all parameters about rotor models. The applied LS estimation approach will be introduced together with the following parameters about aerodynamics.

4.1.2 *Flight test*

After the identification of the above rotor models, the flight test for the quad-TRUAV focuses on the unknown parameters about aerodynamics in the RHSs of (4).

To estimate these parameters, the aerodynamic coefficients $C_\mathcal{D}$, $C_\mathcal{S}$, $C_\mathcal{L}$, $C_\mathcal{R}$, $C_\mathcal{P}$, and $C_\mathcal{Y}$ are required. Based on the measurement outputs $\boldsymbol{y}$ from onboard sensors, the states $\boldsymbol{x}$ in (1) can be assigned. With the recorded control inputs $\boldsymbol{u}$ and rotor models (24), rotor thrusts $F_{\rm r}(\omega_i)$ and reaction torques $Q_{\rm r}(\omega_i)$ $(i = 1, \ldots, 4)$ can be calculated to formulate forces $[F_{{\rm r}x}\ F_{{\rm r}y}\ F_{{\rm r}z}]^{\rm T}$ and moments $[M_{Fx} + M_{Qx}\ M_{Fy}\ M_{Fz} + M_{Qz}]^{\rm T}$ according to (5). Consequently, varying aerodynamic forces and moments can also be calculated. For example, the drag is calculated as follows with (1) and (2):

$$1/2 \cdot \rho V^2 S C_\mathcal{D} = -m\dot{V} - mg \cdot (\cos\alpha\cos\beta\sin\theta - \sin\beta\sin\phi\cos\theta - \sin\alpha\cos\beta\cos\phi\cos\theta) + F_{{\rm r}x}. \tag{27}$$

In every discrete-time sampling instant with $t = kT$, the time-varying coefficients $C_\mathcal{D}(kT)$, $C_\mathcal{S}(kT)$, $C_\mathcal{L}(kT)$, $C_\mathcal{R}(kT)$, $C_\mathcal{P}(kT)$, and $C_\mathcal{Y}(kT)$ are available. Because the pre-processing can be applied to reduce measurement noises offline, the derivatives of states in (27) can be calculated by the Euler approximation. The flight data from the experiment shown in Figure 5 and parameters in airplane mode are applied for the above calculations, and the pre-processing based on the wavelet is used to remove noises partly (refer to the website[2]) for more details).

According to the linear forms in (4), the following equation can be formulated similar to (26) by considering the data in N sampling periods:

$$\boldsymbol{A}_\dagger \boldsymbol{c}_\dagger = \boldsymbol{b}_\dagger, \tag{28}$$

where the subscript $\dagger$ represents $\mathcal{D}$, $\mathcal{S}$, $\mathcal{L}$, $\mathcal{R}$, $\mathcal{P}$, or $\mathcal{Y}$ for different aerodynamic forces or moments, $\boldsymbol{c}_\dagger \in \mathbb{R}^3$ includes all unknown parameters in the RHSs of (4), $\boldsymbol{A}_\dagger \in \mathbb{R}^{N\times 3}$, and $\boldsymbol{b}_\dagger = [C_\dagger(T)\ \cdots\ C_\dagger(NT)]^{\rm T}$.

4.1.3 *Least squares estimation*

In the above contents, some equations about the unknown parameters of the quad-TRUAV have been formulated, as shown by (26) and (28). Because the magnitude of N is absolutely larger than the number of unknown parameters, these equations are all over-determined as follows:

$$\boldsymbol{A}_* \boldsymbol{c}_* = \boldsymbol{b}_*, \tag{29}$$

where $\boldsymbol{A}_* = [\boldsymbol{a}_*(T)\ \cdots\ \boldsymbol{a}_*(NT)]^{\rm T}$ is a matrix, $\boldsymbol{a}_*(kT) \in \mathbb{R}^n$ is a column vector, n is the number of unknown parameters with $N \gg n$, $\boldsymbol{b}_* = [b_*(T)\ \cdots\ b_*(NT)]^{\rm T} = [\tilde{b}_*(T)\ \cdots\ \tilde{b}_*(NT)]^{\rm T} + [\nu(T)\ \cdots\ \nu(NT)]^{\rm T}$

2) https://www.mathworks.com/help/wavelet/ref/wden.html.

is a column vector, $b_*(kT)$ is the measurement value, $\nu(kT)$ is the unavoidable measurement noise, and subscript $*$ represents F, Q, $\mathcal{D}$, $\mathcal{S}$, $\mathcal{L}$, $\mathcal{R}$, $\mathcal{P}$, or $\mathcal{Y}$ for different parameters.

Solving an over-determined equation based on LS approach is the most convenient and widely-used idea [18, 19, 23]. The LS estimations for the unknown parameters in (29) are as follows [10]:

$$\begin{aligned}
\hat{\boldsymbol{c}}_* &= (\boldsymbol{A}_*^{\mathrm{T}}\boldsymbol{A}_*)^{-1}\boldsymbol{A}_*^{\mathrm{T}}\boldsymbol{b}_* = \left[\sum_{k=1}^{N}\boldsymbol{a}_*(kT)\boldsymbol{a}_*^{\mathrm{T}}(kT)\right]^{-1}\sum_{k=1}^{N}\boldsymbol{a}_*(kT)\boldsymbol{b}_*(kT),\\
\hat{\boldsymbol{\sigma}}^2 &= 1/(N-n)\cdot(\boldsymbol{A}_*^{\mathrm{T}}\boldsymbol{A}_*)^{-1}(\boldsymbol{b}_*-\boldsymbol{A}_*\hat{\boldsymbol{c}}_*)^{\mathrm{T}}(\boldsymbol{b}_*-\boldsymbol{A}_*\hat{\boldsymbol{c}}_*),
\end{aligned} \tag{30}$$

where $\hat{\boldsymbol{c}}_*$ is the estimated parameter vector, and $\hat{\boldsymbol{\sigma}}^2$ is the estimated covariance matrix. Note that the above estimations are affected by measurement noises. The difference between the above result $\hat{\boldsymbol{c}}_*$ and estimation without measurement noises $\hat{\hat{\boldsymbol{c}}}_*$ can be represented as follows:

$$\hat{\boldsymbol{c}}_* - \hat{\hat{\boldsymbol{c}}}_* = \left[1/N\sum_{k=1}^{N}\boldsymbol{a}_*(kT)\boldsymbol{a}_*^{\mathrm{T}}(kT)\right]^{-1}\cdot 1/N\sum_{k=1}^{N}\boldsymbol{a}_*(kT)\nu(kT), \tag{31}$$

which means that to ensure the consistence $\hat{\boldsymbol{c}}_* \to \hat{\hat{\boldsymbol{c}}}_*$ is satisfied with $N \to +\infty$, the expectation $\mathrm{E}[\boldsymbol{a}_*(kT)\boldsymbol{a}_*^{\mathrm{T}}(kT)]$ should be nonsingular, and the expectation $\mathrm{E}[\boldsymbol{a}_*(kT)\nu(kT)]$ should be equal to $\mathbf{0}$ [10].

In most cases, the nonsingular $\mathrm{E}[\boldsymbol{a}_*(kT)\boldsymbol{a}_*^{\mathrm{T}}(kT)]$ is usually satisfied. If measurement noises are all Gaussian white noises, $\mathrm{E}[\boldsymbol{a}_*(kT)\nu(kT)] = \mathbf{0}$ will also be satisfied. However, Gaussian white measurement noises are impossible in real applications, so the estimation biases between $\hat{\boldsymbol{c}}_*$ and $\hat{\hat{\boldsymbol{c}}}_*$ are always existing. Some closed-loop identification methods, such as the method based on the instrumental variable (IV) [32], can reduce the estimation biases from measurement noises or closed-loop data. Nonetheless, most closed-loop identification methods focus on the linear model between control inputs and measurement outputs, which are not directly suitable for the nonlinear model identification of the quad-TRUAV. Because estimation biases increase the model mismatches between the nominal model and real system intuitively, the following active model method is still suitable to improve the accuracy of the model.

4.2 Active model method

In the above contents, a nominal nonlinear model of the quad-TRUAV is formulated and identified, which describes the quad-TRUAV dynamics with some accuracy. Model errors with the active model method can accommodate all model mismatches and improve the accuracy of the nonlinear model.

Eq. (6) proposes the model-error-enhanced model of the quad-TRUAV in the continuous-time form. To estimate model mismatches therein with UKF, (6) should be discretized as (23) as follows:

$$\boldsymbol{x}_k = \boldsymbol{x}_{k-1} + \int_{(k-1)T}^{kT}\boldsymbol{f}_{\mathrm{c}}(\boldsymbol{x}(t),\boldsymbol{u}(t))\mathrm{d}t + \boldsymbol{E}\int_{(k-1)T}^{kT}\boldsymbol{e}_{\mathrm{c}}(t)\mathrm{d}t, \quad \boldsymbol{y}_k = \boldsymbol{x}_k. \tag{32}$$

Because the sampling period T is very small in flight experiments ($T = 0.008$ s according to the quad-TRUAV dynamics), the following discrete-time forms are obtained with approximations:

$$\boldsymbol{f}(\boldsymbol{x}_{k-1},\boldsymbol{u}_{k-1}) \approx \boldsymbol{x}_{k-1} + T\cdot\boldsymbol{f}_{\mathrm{c}}(\boldsymbol{x}(kT-T),\boldsymbol{u}(kT-T)), \quad \boldsymbol{e}_{k-1} \approx T\cdot\boldsymbol{e}_{\mathrm{c}}(kT-T), \tag{33}$$

which will be applied in the following contents. Without some prior knowledge about model errors, $\boldsymbol{e}_k$ in (23) is assumed as the stationary random process and driven by a process noise vector $\boldsymbol{w}_k$ [20–23]:

$$\boldsymbol{e}_k = \boldsymbol{e}_{k-1} + \boldsymbol{w}_{k-1}. \tag{34}$$

With the above assumption, the active model method usually forms a proportional-integral observer to estimate the slowly varying parts of model errors mainly, and some high-frequency parts have to be ignored.

Table 2 Estimated parameters of quad-TRUAV nonlinear model

Parameter	Estimated values	Estimated standard deviations
$\hat{a}_0$, $\hat{a}_1$, $\hat{a}_2$	−0.640, 1.832, −2.189	0.0054, 0.0100, 0.0054
$\hat{b}_0$, $\hat{b}_1$, $\hat{b}_2$, $\hat{b}_3$	−0.0011, 0.0024, −0.0024, 0.0012	4.9×10^{-5}, 1.3×10^{-4}, 1.3×10^{-4}, 4.9×10^{-5}
$\hat{\overline{K}}$	0.126	3.973×10^{-5}
$\hat{C}_{\mathcal{D}0}$, $\hat{C}_{\mathcal{D}1}$, $\hat{C}_{\mathcal{D}2}$	0.573, 2.004, 6.060	0.0302, 0.665, 3.518
$\hat{C}_{\mathcal{S}1}$, $\hat{C}_{\mathcal{S}p}$, $\hat{C}_{\mathcal{S}r}$	0.289, −0.264, 4.642	0.0078, 0.189, 0.190
$\hat{C}_{\mathcal{L}0}$, $\hat{C}_{\mathcal{L}1}$, $\hat{C}_{\mathcal{L}q}$	0.780, 2.337, 14.076	0.0096, 0.0940, 2.337
$\hat{C}_{\mathcal{R}1}$, $\hat{C}_{\mathcal{R}p}$, $\hat{C}_{\mathcal{R}r}$	−0.0686, −0.405, 0.8713	0.0026, 0.0634, 0.0640
$\hat{C}_{\mathcal{P}0}$, $\hat{C}_{\mathcal{P}1}$, $\hat{C}_{\mathcal{P}q}$	−0.0312, −0.628, −3.349	0.0025, 0.0243, 0.604
$\hat{C}_{\mathcal{Y}1}$, $\hat{C}_{\mathcal{Y}p}$, $\hat{C}_{\mathcal{Y}r}$	0.0424, 0.391, 0.626	0.0015, 0.0355, 0.0358

Based on (23) and (34), the following augmented system is formulated:

$$\begin{bmatrix} \boldsymbol{x}_k \\ \boldsymbol{e}_k \end{bmatrix} = \begin{bmatrix} \boldsymbol{f}(\boldsymbol{x}_{k-1}, \boldsymbol{u}_{k-1}) + \boldsymbol{E}\boldsymbol{e}_{k-1} \\ \boldsymbol{e}_{k-1} \end{bmatrix} + \begin{bmatrix} \boldsymbol{v}_{k-1} \\ \boldsymbol{w}_{k-1} \end{bmatrix} \triangleq \boldsymbol{f}^{\mathrm{a}}(\boldsymbol{x}_k^{\mathrm{a}}, \boldsymbol{u}_k) + \boldsymbol{\mu}_k, \tag{35}$$

where $\boldsymbol{x}_k^{\mathrm{a}} = [\boldsymbol{x}_k^{\mathrm{T}}\ \boldsymbol{e}_k^{\mathrm{T}}]^{\mathrm{T}}$ is the augmented state vector, and $\boldsymbol{\mu}_k = [\boldsymbol{v}_k^{\mathrm{T}}\ \boldsymbol{w}_k^{\mathrm{T}}]^{\mathrm{T}}$ is the process noise vector with $\boldsymbol{v}_k$ as the process noise vector of (23). Furthermore, the following measurement equation is defined:

$$\boldsymbol{y}_k = \boldsymbol{x}_k + \boldsymbol{\nu}_k = \boldsymbol{h}^{\mathrm{a}}(\boldsymbol{x}_k^{\mathrm{a}}) + \boldsymbol{\nu}_k, \tag{36}$$

where only the measurement outputs about flight states are included, and $\boldsymbol{\nu}_k$ is the measurement noise vector. Eqs. (35) and (36) form the nonlinear system for online estimation.

To apply UKF for the estimations of $\boldsymbol{x}_k$ and $\boldsymbol{e}_k$ simultaneously, process and measurement noises are assumed as the Gaussian white noises satisfying $\mathrm{Cov}(\boldsymbol{\mu}_k, \boldsymbol{\mu}_j) = \boldsymbol{Q}\boldsymbol{\delta}_{kj}$, $\mathrm{Cov}(\boldsymbol{\nu}_k, \boldsymbol{\nu}_j) = \boldsymbol{R}\boldsymbol{\delta}_{kj}$, and $\mathrm{Cov}(\boldsymbol{\mu}_k, \boldsymbol{\nu}_j) = \boldsymbol{0}$, where $\boldsymbol{Q}$ and $\boldsymbol{R}$ are the covariance matrices of the noises, $\boldsymbol{\delta}_{kj} = \boldsymbol{0}$ when $k \neq j$, and $\boldsymbol{\delta}_{kj}$ is an identity matrix when $k = j$. For the quad-TRUAV system, $\boldsymbol{y}_k \in \mathbb{R}^{10}$ and $\boldsymbol{x}_k^{\mathrm{a}} \in \mathbb{R}^{16}$, where $\boldsymbol{e}_k \in \mathbb{R}^6$ is considered only for dynamic equations, whose accuracy is reduced by model mismatches directly.

5 Model validation based on flight data

With the control method in Figure 3, flight experiments are conducted before the model identification to collect flight data, as shown in Figure 5. With the ground test and flight data, LS approach is applied to obtain the estimated parameters and estimated standard deviations in Table 2. In the case without measurement noises or with only Gaussian white noises, by representing the estimated value as $\hat{c}$ and its estimated standard deviation as $\hat{\sigma}(\hat{c})$, $\hat{c} \pm 1.96\hat{\sigma}(\hat{c})$ is a good approximation for the 95% confidence interval. Based on this criterion, the estimations in Table 2 provide good confidence. To validate the above study, the following contents will display some flight experiment results. Then real data are applied to validate the identified nominal model and model-error-enhanced model of the quad-TRUAV.

5.1 Flight experiment results

In the flight experiments with the control structure designed in Section 3, the quad-TRUAV takes off vertically, and tilts rotors at $\pi/4$ rad for acceleration. When the flight velocity is larger than the stalling speed 7 m/s, the quad-TRUAV tilts into airplane mode and cruises to record enough flight data, as shown in Figure 6. Without velocity and height controllers, the flight velocity and height fluctuate under the control instructions from the ground control station. To reduce the bad effect from external interferences for data collection, the degree of wind is required not more than Beaufort two. A video about flight experiments is presented in the website[3)].

Furthermore, Figure 7 displays the curves of Euler angles and attitude rates from a set of flight data, where attitude references are provided by the ground control station, and attitude rate references are calculated by the attitude controller block shown in Figure 3 corresponding to $\boldsymbol{\mathcal{K}} \cdot (\boldsymbol{\eta}_{\mathrm{d}} - \boldsymbol{\eta})$ in (22). These curves display the effectiveness of the designed control method. Note that the reference value of

3) https://v.qq.com/x/page/w0976sg2kof.html.

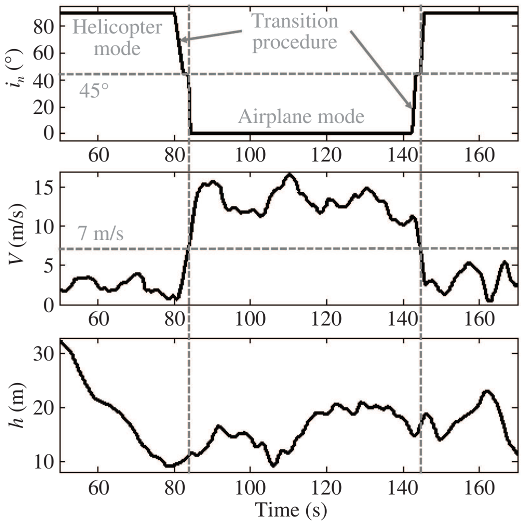

Figure 6 (Color online) Average rotor-tilt angle, flight velocity, and flight height in an experiment.

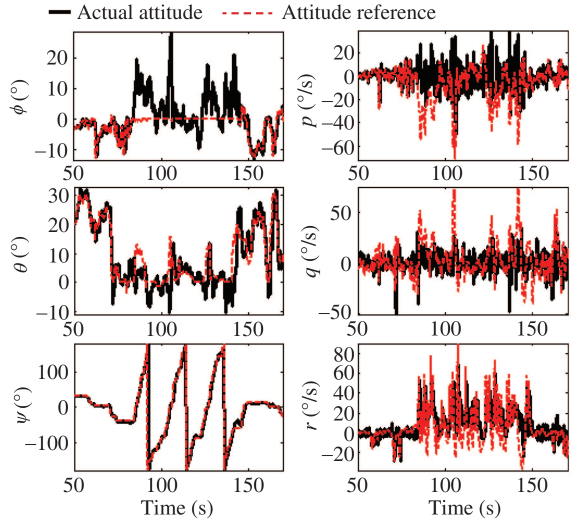

Figure 7 (Color online) Euler angles and attitude rates in a flight experiment.

ϕ is almost zero in airplane mode. However, due to the dynamic coupling between rolling and yawing motions, ϕ is accompanied with fluctuations with the variations of ψ.

5.2 Quad-TRUAV model validation

The nominal model of the quad-TRUAV is identified with the nonlinear equations (1)–(5), rotor models (24), and estimated parameters listed in Table 2. Based on some modeling assumptions and real flight data, this nominal model is approximate and also a typical model from offline system identification methods as the models in [6, 9]. By representing it as $\hat{\boldsymbol{x}}_k = \hat{\boldsymbol{f}}(\boldsymbol{x}_{k-1}, \boldsymbol{u}_{k-1})$, $\hat{\boldsymbol{x}}_k$ means the one-step predicted state vector with $\boldsymbol{x}_{k-1} = \boldsymbol{y}_{k-1}$. For the further accuracy of the model, the active model method with UKF is applied to estimate model errors based on the augmented system (35) and (36). The parameters for UKF are mainly based on heuristic knowledge, and set as $\boldsymbol{Q} = \mathrm{diag}(0.1, 0.1, 0.01, 1, 0.01, 0.01, 1, 1, 0.01, 0.01, 1, 1, 1, 1, 1, 1)$, $\boldsymbol{R} = \mathrm{diag}(0.1, 0.1, 0.01, 1, 0.01, 0.01, 1, 1, 0.01, 0.01)$, $\alpha_{\mathrm{UKF}} = 1$, and $\beta_{\mathrm{UKF}} = 2$.

To validate the quad-TRUAV models sufficiently, fresh flight data in different flight modes are considered to compare actual states and their predicted values from different models. With the measurement outputs $\boldsymbol{y}_k$ from onboard sensors and the control inputs $\boldsymbol{u}_k$ recorded by the Pixhawk, the M-step predicted state vector by the moving-horizon (prediction from the nominal model)

$$\hat{\boldsymbol{x}}_k = \hat{\boldsymbol{f}}(\hat{\boldsymbol{x}}_{k-1}, \boldsymbol{u}_{k-1}) \tag{37}$$

will be displayed, where $\hat{\boldsymbol{x}}_{k-1} = \hat{\boldsymbol{f}}(\hat{\boldsymbol{x}}_{k-2}, \boldsymbol{u}_{k-2})$, ..., and $\hat{\boldsymbol{x}}_{k-M+1} = \hat{\boldsymbol{f}}(\boldsymbol{y}_{k-M}, \boldsymbol{u}_{k-M})$. With the model error estimation $\hat{\boldsymbol{e}}_k$ from UKF, the M-step prediction from the model-error-enhanced model

$$\hat{\tilde{\boldsymbol{x}}}_k = \hat{\boldsymbol{f}}(\hat{\tilde{\boldsymbol{x}}}_{k-1}, \boldsymbol{u}_{k-1}) + \boldsymbol{E}\hat{\boldsymbol{e}}_{k-1} \tag{38}$$

will also be shown, where $\hat{\tilde{\boldsymbol{x}}}_{k-1} = \hat{\boldsymbol{f}}(\hat{\tilde{\boldsymbol{x}}}_{k-2}, \boldsymbol{u}_{k-2}) + \boldsymbol{E}\hat{\boldsymbol{e}}_{k-2}$, ..., and $\hat{\tilde{\boldsymbol{x}}}_{k-M+1} = \hat{\boldsymbol{f}}(\boldsymbol{y}_{k-M}, \boldsymbol{u}_{k-M}) + \boldsymbol{E}\hat{\boldsymbol{e}}_{k-M}$. Figure 8 displays and compares the actual states in different flight modes with their M-step predictions from (37) and (38). To compromise the model validation and computation time, M is set as 5 in these curves. The prediction errors $\hat{\boldsymbol{x}}_k - \boldsymbol{x}_k$ and $\hat{\tilde{\boldsymbol{x}}}_k - \boldsymbol{x}_k$ of all states are also shown, and their absolute averages are listed in Table 3, where the absolute average of signal $\tau(t)$ is defined as $\mathrm{ave}(|\tau(t)|) = 1/N \sum_{k=1}^{N} |\tau(kT)|$, the values with " $\hat{}$ " are from (37), and the values with " $\hat{\tilde{}}$ " are from (38).

According to Figure 8 and Table 3, the kinematic models about h and $[\phi\ \theta\ \psi]^{\mathrm{T}}$ are all with excellent accuracy. It it rational because there is no unknown parameter in kinematic equations. However, the nominal dynamic model presents different accuracy in different flight modes, which is mainly caused by modeling assumptions and some other inaccuracy. Especially during the transition procedure, the

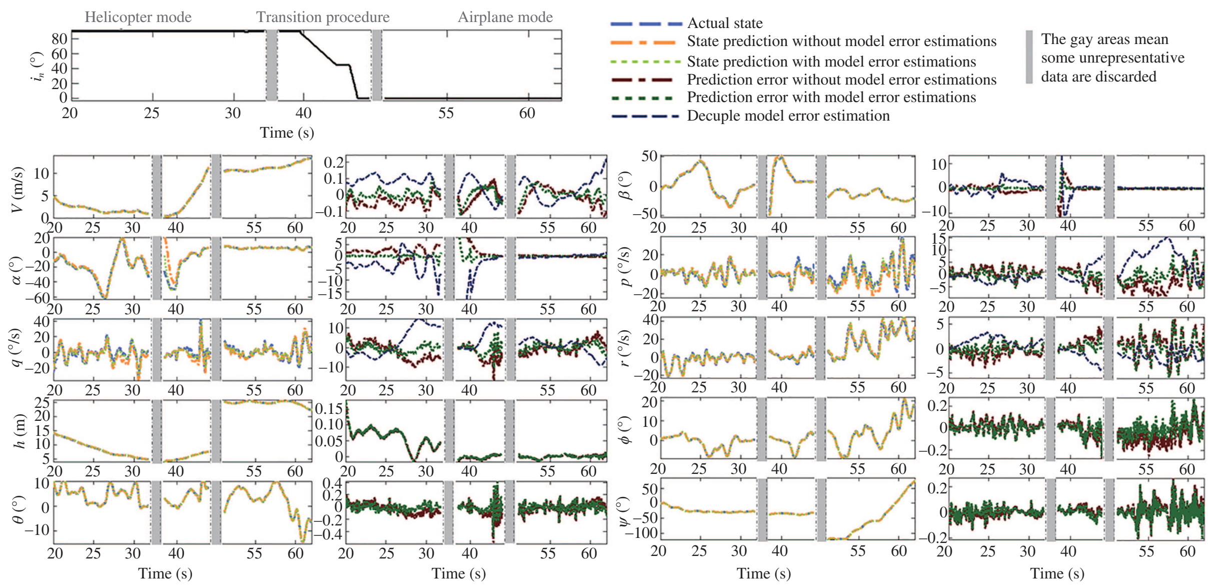

Figure 8 (Color online) Quad-TRUAV model validation with three sets of flight data and M-step predictions ($M = 5$).

Table 3 Absolute averages of M-step prediction errors (with the same units as Figure 8)

	Helicopter mode	Transition procedure	Airplane mode		Helicopter mode	Transition procedure	Airplane mode
ave($\lvert\hat{V} - V\rvert$)	0.0451	0.0463	0.0451	ave($\lvert\hat{\beta} - \beta\rvert$)	0.9044	1.2515	0.1407
ave($\lvert\tilde{\hat{V}} - V\rvert$)	0.0213	0.0381	0.0239	ave($\lvert\tilde{\hat{\beta}} - \beta\rvert$)	0.2330	0.3258	0.0361
Increase rate (%)	52.8	17.7	47.0	Increase rate (%)	74.2	73.9	74.3
ave($\lvert\hat{\alpha} - \alpha\rvert$)	2.3140	3.4353	0.2065	ave($\lvert\hat{p} - p\rvert$)	1.5630	2.7496	4.7035
ave($\lvert\tilde{\hat{\alpha}} - \alpha\rvert$)	0.3816	0.5246	0.0509	ave($\lvert\tilde{\hat{p}} - p\rvert$)	1.3400	1.7092	2.7824
Increase rate (%)	83.5	84.7	75.4	Increase rate (%)	14.3	37.8	40.8
ave($\lvert\hat{q} - q\rvert$)	3.8038	4.3009	2.1395	ave($\lvert\hat{r} - r\rvert$)	1.0395	1.3601	2.2137
ave($\lvert\tilde{\hat{q}} - q\rvert$)	1.6365	2.3089	1.5923	ave($\lvert\tilde{\hat{r}} - r\rvert$)	0.7207	0.6629	1.8619
Increase rate (%)	56.9	46.3	25.6	Increase rate (%)	30.7	51.3	15.9
ave($\lvert\hat{h} - h\rvert$)	0.0592	0.0050	0.0039	ave($\lvert\hat{\phi} - \phi\rvert$)	0.0381	0.0549	0.0891
ave($\lvert\tilde{\hat{h}} - h\rvert$)	0.0603	0.0045	0.0036	ave($\lvert\tilde{\hat{\phi}} - \phi\rvert$)	0.0366	0.0442	0.0617
ave($\lvert\hat{\theta} - \theta\rvert$)	0.0682	0.0923	0.0526	ave($\lvert\hat{\psi} - \psi\rvert$)	0.0202	0.0242	0.0493
ave($\lvert\tilde{\hat{\theta}} - \theta\rvert$)	0.0396	0.0692	0.0474	ave($\lvert\tilde{\hat{\psi}} - \psi\rvert$)	0.0198	0.0233	0.0427

nominal models about α, q, and β are less accurate than them in other flight modes, and the nominal models about p and r are also worse than them in helicopter mode.

To accommodate the above model mismatches, model errors are estimated for dynamic states, and their decuple values are shown in Figure 8, which present obvious correlations with prediction errors. Compared to the identified nominal model, which is also a typical nonlinear model from offline system identification methods, the model-error-enhanced model is more accurate, as shown by the increase rates about dynamic states listed in Table 3. The above results mean the active model-based nonlinear system identification improves the quad-TRUAV model, and the accuracy and complexity of the model are compromised by additional model errors and a less complex nominal model. However, limited by the assumed model (34), active model methods in this study and other references [20–23] can not estimate some time-varying parts of model errors. For excellent TRUAV models, time-varying model error estimation methods are worth considering and comparing with current propositions.

6 Conclusion

This paper focuses on the active model-based nonlinear system identification of quad-TRUAV. According to some modeling assumptions, the quad-TRUAV nominal model is formulated in a nonlinear and relatively concise form. Based on the simplification of the model, IDA-PBC is applied to attitude control and flight experiments of quad-TRUAV. Some unknown parameters in the nominal model are estimated offline based on real flight data. To improve the accuracy of the model, an active model method using UKF is developed to estimate model errors online. According to numerical results, the designed control method ensures the attitude stability of quad-TRUAV in all flight modes. The identified nominal model describes the TRUAV dynamics in a less complex form, and the estimated model errors further improve the accuracy of the model. The accuracy and complexity of the model are effectively compromised.

In future work, the active model method for quad-TRUAV will be further modified. Estimating some time-varying model errors improves the accuracy of the model-error-enhanced model. In addition, the quad-TRUAV flight control enhanced by model errors will be investigated. By introducing an integrated nonlinear model, the model-error-enhanced control provides better control performance than current methods that rely on nominal models.

Acknowledgements This work was supported by the Major Research Program of National Natural Science Foundation of China (Grant No. 91748130), National Natural Science Foundation of China (Grant No. U1608253), and Chinese Academy of Sciences (Grant No. 6141A01061601).

References

1 Liu Z, He Y Q, Yang L Y, et al. Control techniques of tilt rotor unmanned aerial vehicle systems: a review. Chin J Aeronaut, 2017, 30: 135–148
2 Ferguson S W. A mathematical model for real time flight simulation of a generic tilt-rotor aircraft. NASA CR-166536. 1988
3 Ye L, Zhang Y, Yang S, et al. Numerical simulation of aerodynamic interaction for a tilt rotor aircraft in helicopter mode. Chin J Aeronaut, 2016, 29: 843–854
4 Du S L, Wang C, Sun H J, et al. Numerical analysis of aerodynamic interference of rotor/fuselage in transition state of tilting four-rotor UAV. J Nanjing Univ Aeronaut Astronaut, 2018, 50: 179–185
5 Chen K, Shi Z W, Tong S X, et al. Aerodynamic interference test of quad tilt rotor aircraft in wind tunnel. Proc I Mech Eng Part G-J Aer Eng, 2019, 233: 5553–5566
6 Papachristos C, Alexis K, Tzes A. Dual-authority thrust-vectoring of a tri-tiltrotor employing model predictive control. J Intell Robot Syst, 2016, 81: 471–504
7 Cardoso D N, Esteban S, Raffo G V. A nonlinear W_∞ controller of a tilt-rotor UAV for trajectory tracking. In: Proceedings of European Control Conference (ECC), Napoli, 2019. 928–934
8 Yuksek B, Vuruskan A, Ozdemir U, et al. Transition flight modeling of a fixed-wing VTOL UAV. J Intell Robot Syst, 2016, 84: 83–105
9 Chen C. Research on control method for the transition model of the small tilt-rotor UAV. Dissertation for Ph.D. Degree. Changsha: National University of Defense Technology, 2017
10 Morelli E A, Klein V. Aircraft System Identification: Theory and Practice. Williamsburg: Sunflyte Enterprises, 2016
11 Liu Z, Theilliol D, Yang L Y, et al. Transition control of tilt rotor unmanned aerial vehicle based on multi-model adaptive method. In: Proceedings of International Conference on Unmanned Aircraft Systems (ICUAS), Miami, 2017. 560–566
12 Wang Z G, Li J B, Duan D Y. Manipulation strategy of tilt quad rotor based on active disturbance rejection control. Proc Inst Mech Eng Part G-J Aerospace Eng, 2020, 234: 573–584
13 Muscarello V, Colombo F, Quaranta G, et al. Aeroelastic rotorcraft-pilot couplings in tiltrotor aircraft. J Guidance Control Dyn, 2019, 42: 524–537
14 Liu Z, Theilliol D, Yang L Y, et al. Observer-based linear parameter varying control design with unmeasurable varying parameters under sensor faults for quad-tilt rotor unmanned aerial vehicle. Aerosp Sci Tech, 2019, 92: 696–713
15 Hartmann P, Meyer C, Moormann D. Unified velocity control and flight state transition of unmanned tilt-wing aircraft. J Guidance Control Dyn, 2017, 40: 1348–1359
16 Liu Z, Theilliol D, He Y Q, et al. Interconnection and damping assignment passivity-based control design under loss of actuator effectiveness. J Intell Robot Syst, 2020, 100: 29–45
17 Donaire A, Romero J G, Ortega R, et al. Robust IDA-PBC for underactuated mechanical systems subject to matched disturbances. Int J Robust nonlinear Control, 2017, 27: 1000–1016
18 Han W X, Wang Z H, Shen Y. Fault estimation for a quadrotor unmanned aerial vehicle by integrating the parity space approach with recursive least squares. Proc I Mech Eng Part G-J Aer Eng, 2018, 232: 783–796
19 Cui J, Lai M, Chu Z Y, et al. Experiment on impedance adaptation of under-actuated gripper using tactile array under unknown environment. Sci China Inf Sci, 2018, 61: 122202
20 Li B B, He Y Q, Han J D, et al. A new modeling scheme for powered parafoil unmanned aerial vehicle platforms: theory and experiments. Chin J Aeronaut, 2019, 32: 2466–2479
21 Yi K, Liang X, He Y Q, et al. Active-model-based control for the quadrotor carrying a changed slung load. Electronics, 2019, 8: 461
22 Zhang D H, Zhao X G, Han J D. Active model-based control for pneumatic artificial muscle. IEEE Trans Ind Electron, 2017, 64: 1686–1695
23 Han J D, Xiong J F, He Y Q, et al. Nonlinear modeling for a water-jet propulsion USV: an experimental study. IEEE Trans Ind Electron, 2017, 64: 3348–3358
24 Wan E A, Merwe R V D. The unscented kalman filter for nonlinear estimation. In: Proceedings of Adaptive Systems for Signal Processing, Communications, and Control Symposium, Alberta, 2000. 1–6
25 Krznar M, Kotarski D, Piljek P, et al. On-line inertia measurement of unmanned aerial vehicles using on board sensors and bifilar pendulum. Interdiscip Descr Complex Syst, 2018, 16: 149–161
26 Robert F S. Flight Dynamics. Princeton: Princeton University Press, 2004
27 Khalil H K. Nonlinear Systems. 3rd ed. New Jersey: Prentice Hall, 2002
28 Yuan Y, Cheng L, Wang Z D, et al. Position tracking and attitude control for quadrotors via active disturbance rejection control method. Sci China Inf Sci, 2019, 62: 010201
29 Chen C, Zhang J Y, Zhang D B, et al. Control and flight test of a tilt-rotor unmanned aerial vehicle. Int J Adv Robotic Syst, 2017, 14: 172988141667814
30 He T P, Liu H, Li S. Quaternion-based robust trajectory tracking control for uncertain quadrotors. Sci China Inf Sci, 2016, 59: 122902
31 Qi X. The research on fault-tolerant control and re-planning for unmanned aerial vehicles. Dissertation for Ph.D. Degree. Shenyang: Shenyang Institute of Automation, Chinese Academy of Sciences, 2017
32 Brunot M, Janot A, Young P C, et al. An improved instrumental variable method for industrial robot model identification. Control Eng Practice, 2018, 74: 107–117